Physics of Fluids ARTICLE pubs.aip.org/aip/pof

# Computational fluid dynamics simulations of the heat transfer properties of graphene-based nanolubricants and application to hydrodynamic lubrication

Cite as: Phys. Fluids **36**, 053106 (2024); doi: 10.1063/5.0193228
Submitted: 21 December 2023 · Accepted: 9 April 2024 ·
Published Online: 9 May 2024



Roberto Guarino[1,a] and Nicola Maria Pugno[1,2,b]

## AFFILIATIONS

[1]Laboratory of Bio-Inspired, Bionic, Nano, Meta Materials & Mechanics, Department of Civil, Environmental and Mechanical Engineering, University of Trento, via Mesiano 77, 38123 Trento, Italy
[2]School of Engineering and Materials Science, Queen Mary University of London, Mile End Road, E1-4NS London, United Kingdom

[a]**Present address:** École Polytechnique Fédérale de Lausanne (EPFL), Swiss Plasma Center (SPC), PSI, Villigen CH-5232, Switzerland.
[b]**Author to whom correspondence should be addressed:** nicola.pugno@unitn.it

## ABSTRACT

In this paper, we consider experimental data available for graphene-based nanolubricants to evaluate their convective heat transfer performance by means of computational fluid dynamics (CFD) simulations. Single-phase models with temperature-dependent properties are employed for this purpose. The base fluid is a polyalkylene glycol, and we show the effect of the addition of carbon nanohorns and graphene nanoplatelets (GNPs), in different volume fractions, on the convective heat transfer coefficient between two parallel plates. Then, an application to hydrodynamic lubrication is discussed. The extreme in-plane thermal conductivity of graphene allows a smaller temperature rise of the GNP-based nanolubricant, i.e., a more effective heat removal. To the best of our knowledge, this work represents the first application of single-phase nanofluid models to hydrodynamic lubrication.





## I. INTRODUCTION

Nanofluids are stable colloidal suspensions obtained by adding nanometer-sized particles to a base fluid and present novel rheological and heat transfer properties that can be exploited in many engineering fields. In recent years, the use of nanoparticles for the functionalization of fluids has acquired a growing interest in tribology. In fact, thanks to their superior thermal, frictional, and anti-wear properties, nanolubricants are demonstrated to be potentially critical in a variety of tribological applications, principally when a low coefficient of friction, a reduced wear rate, and/or an large heat removal is required.

Within this frame, carbon-based materials, such as graphene, graphene oxide (GO), carbon nanotubes (CNTs), carbon nanohorns (CNHs), and carbon nano-onions (CNOs) as dispersed phases in nanofluids are extremely interesting and have been the object of several experimental investigations.[1–12] The most significant properties of the resulting suspensions that have been observed are a non-Newtonian rheological behavior and an increased thermal conductivity.[13] From the tribological point of view, the lubricating properties, e.g., of graphite and two-dimensional (2D) materials (e.g., graphene) are well-known in dry contacts,[14] but they are demonstrated to be exceptional candidates also as lubricant additives. In this case, more than a reduced coefficient of friction (generally in the range 5%–30%), the most relevant effect is the wear reduction of the surfaces in contact. More in general, the use of carbon-based materials for loading nanofluids has a relevant technological interest in several fluid dynamics-related domains.[15–18]

The numerical simulations of fluid flow and heat transfer in nanofluids are generally carried out following two alternative approaches: single- or two-phase modeling.[19–21] Single-phase models for particle suspensions in fluids are based on a continuum representation of the nanofluid, which is considered a standard fluid with effective properties (as a function of the nanoparticle volume fraction). The main idea behind single-phase modeling is that the nanoparticles move exactly at the same velocity as the base fluid and are in thermal equilibrium with the surrounding medium. This approach is justified by a very small Stokes number Stk of the suspension, which leads to

acceptable results in many heat transfer and fluid flow applications. Specifically, the value of Stk is given by

$$\mathrm{Stk} = \frac{t_o u_0}{l_0}, \tag{1}$$

where $t_0$ is the characteristic relaxation time of the particle, and $u_0$ and $l_0$ are the reference flow velocity and the characteristic flow length, respectively.

Several approaches exist to compute the effective physical properties of a nanofluid, and one of the first ideas was proposed by Einstein.[22] In two-phase models, instead, the nanoparticles are taken into account as a separate phase mixed with the base fluid. The idea behind this approach is mainly related to a possible non-zero slip velocity between each particle and the surrounding fluid; thus, the conservation equations are those employed for mixtures. Many authors claim a higher accuracy of two-phase models, but at the cost of an increased complexity and computational expense.

Several works in the literature deal with the computational treatment of nanofluids, but only a few papers are focused specifically on graphene and, in general, on carbon-based nanolubricants. For instance, Amiri *et al.*[23] present a computational fluid dynamics (CFD) study on the heat transfer properties of functionalized graphene nanoplatelet (GNP)-based nanofluids over a backward facing step. By employing single-phase models at constant temperature, the authors show the effect of the nanoparticle volume fraction on the convective heat transfer coefficient and on some recirculation phenomena driven by the geometry. Khaliq *et al.*,[24] instead, show the effect of graphene nanoflake content on the efficiency of polymerase chain reaction. To this end, they employ also single-phase CFD simulations to study the improved thermal performance of the nanofluid with respect to the base fluid. In all the cases, the modeling of the rheology of the nanofluid, especially the correct estimation of the viscosity, results to be fundamental for a quantitative description of the physical phenomena.

Shahmohamadi *et al.*[25] use a Lagrangian model with cavitation to evaluate the thermal and frictional performance of a nanolubricant with respect to the base fluid. They show the improved heat transfer properties of the nanofluid, while no significant friction reduction is observed numerically. The presented analysis is carried out only for a specific nanolubricant formulation, i.e., for only one nanoparticle volume fraction.

Despite the above-mentioned works in the literature, to the best of our knowledge, a CFD study of the tribological (i.e., frictional) properties of carbon-based nanolubricants is still missing. As reported above, indeed, almost all the CFD literature on nanofluids is focused on the modeling of the effective properties and/or of the thermal behavior. The main novelty of this work, in fact, is the study of the hydrodynamic lubrication in the case of a very simple geometry (i.e., the plane slider bearing) with a focus on the enhancement of the load-carrying capacity and the reduction in sliding friction thanks to the loading of nanofluids with different volume fractions of nanoparticles.

A first objective of the present work is to quantitatively describe the convective heat transfer properties of graphene-based nanolubricants, with a particular focus on their exploitation in hydrodynamic lubrication. We employ single-phase nanofluid models to derive the rheological and thermal properties of the nanolubricants as a function of the nanoparticle volume fraction. Then, we study the convective heat transfer in a confined geometry by means of CFD simulations and extract the convective heat transfer coefficient, considering the temperature dependence of the fluid properties. Finally, we employ this result to study the hydrodynamic lubrication in a plane slider bearing, and we attempt to extract also macroscopic tribological quantities (namely, the load-carrying capacity of the bearing and the coefficient of friction) as a function of the nanoparticle volume fraction.

## II. SINGLE-PHASE MODELING

### A. Base fluid and nanoparticle properties

The base fluid considered here is a polyalkylene glycol (PAG) lubricant, which is largely employed in several industrial applications, such as hydraulic systems, compressors, and gearbox lubrication.[26–28] A peculiarity of PAG lubricants is their large oxygen content, which gives them an intrinsic polarity and can thus affect their interactions with dispersed phases.[29] The main physical properties of the PAG lubricant considered here are listed in Appendix A, where $T$ is the temperature, $\rho$ the density, $c$ the specific heat capacity, $\mu$ the dynamic viscosity, and $k$ the thermal conductivity.

Recently, several PAG nanofluids have been developed,[9,30,31] with the objective of achieving superior thermal and tribological performance. In this work, we consider the nanofluid obtained by CNHs as a dispersed phase, whose main properties are taken from the literature[32] and listed in Table II in Appendix A. Despite CNHs having a very complex shape, here we assume they can be approximated by a sphere with isotropic properties and $r$ denotes the average nanoparticle radius.

In addition to the PAG-CNH nanofluid data available in Ref. 9, we hypothesize also the use of GNPs for the functionalization of the same base fluid. Again, the GNP properties are taken from the literature[33] and listed in Table III in Appendix A. In contrast to CNHs, GNPs present strongly anisotropic mechanical, electrical, and thermal properties; thus, at least two directions (i.e., longitudinal and transversal) must be taken into account. $l$ and $d$ denote the average nanoparticle length and thickness, respectively, while $k_p$ is the in-plane thermal conductivity, here assumed to be equal to the in-plane conductivity of CNTs.

Both in the case of the PAG-CNH and of the PAG-GNP nanolubricant, the following nanoparticle volume fractions $\varphi$ are considered: 0.00% (i.e., the base fluid), 0.05%, 0.10%, 0.25%, and 0.50%.

### B. Effective properties

The effective density and specific heat capacity of the nanolubricants as a function of $\varphi$ are computed by using the following mixture rules:

$$\rho_{\mathrm{eff}} = \rho_b(1-\varphi) + \rho_p\,\varphi, \tag{2}$$

$$\rho_{\mathrm{eff}}\, c_{\mathrm{eff}} = \rho_b\, c_b(1-\varphi) + \rho_p\, c_p\,\varphi, \tag{3}$$

where the subscripts $b$ and $p$ refer to the base fluid and the nanoparticles, respectively.

The Maron–Pierce's model[34] is employed here to model the effective dynamic viscosity of the considered nanolubricants:

$$\frac{\mu_{\mathrm{eff}}}{\mu_b} = \left(1 - \frac{\varphi}{\varphi_M}\right)^{-2}, \tag{4}$$

where $\varphi_M$ has the physical meaning of a maximum volume fraction. For the PAG-CNH nanolubricant, we can introduce a fractal-like nanoparticle aggregation, i.e., the spontaneous formation of clusters,

by substituting $\varphi$ in Eq. (4) with $\varphi_a$, which is an equivalent volume fraction given by[35,36]:

$$\varphi_a = \varphi \left(\frac{r_a}{r}\right)^{3-D}, \tag{5}$$

with $r_a$ being the average cluster radius and $D \approx 1.8$ is taken as fractal index.[36] The resulting modified Maron–Pierce's formula, from Eq. (4), is:

$$\frac{\mu_{\text{eff}}}{\mu_b} = \left[1 - \frac{\varphi}{\varphi_M}\left(\frac{r_a}{r}\right)^{3-D}\right]^{-2}. \tag{6}$$

The experimental data of the viscosity of the PAG-CNH nanofluid are taken from Ref. 9 and the best-fit through Eq. (6), as shown in Fig. 1, gives $\varphi_M \approx 6.6\%$ and $r_a \approx 80$ nm as fitting parameters.

For the PAG-GNP nanolubricant, instead, given the elongated shape of GNPs and thus the difficulty in defining a cluster and a related radius, we do not consider nanoparticle aggregation. Therefore, we employ the original formulation expressed through Eq. (4). In the same figure, we plot the data related to the PAG-GNP nanofluid, whose experimental values are taken from Ref. 33, where, strictly speaking, the authors present an investigation on water-GNP nanofluids. However, in a first approximation and neglecting high-order effects, e.g., due to interactions at the molecular level, we can assume that the addition of nanoparticles has the same effect (i.e., the same law for $\frac{\mu_{\text{eff}}}{\mu_b}$ as a function of $\varphi$) on the macroscopic rheological behavior of the PAG nanolubricant considered in this work. In this case, the best-fit through Eq. (4) gives $\varphi_M \approx 9.6\%$. Note from Fig. 1 that the two nanofluids present very similar values for the effective dynamic viscosity, although the shape of the nanoparticles is different. The single-phase models used here, in fact, do not allow to describe the nanoscale behavior of the suspension, for instance, the orientation of elongated nanoparticles with respect to the direction of shear, despite being suitable for a precise match of the experimental (i.e., macroscopic) data.

For the determination of the effective thermal conductivity of the PAG-CNH nanolubricant, here we employ a simplified Nan's model[37,38]:

$$\frac{k_{\text{eff}}}{k_b} = 1 + \frac{\varphi}{3}\frac{\widehat{k}_p}{k_b}, \tag{7}$$

where the Kapitza resistance $R_K$ (also known as interfacial thermal resistance) is introduced through:

$$\widehat{k}_p = \frac{k_p}{1 + \dfrac{R_K\, k_p}{r}}. \tag{8}$$

The best-fit of the experimental data through Eq. (7), as shown in Fig. 2, gives the combination $R_K \approx 4 \times 10^{-9}\ \text{m}^2\ \text{K W}^{-1}$ and $k_p \approx 45\ \text{W m}^{-1}\ \text{K}^{-1}$, which are reasonable values for a CNH-based composite, as found elsewhere.[39]

In order to model the effective thermal conductivity of the PAG-GNP nanolubricant, instead, the anisotropic thermal properties of the graphene nanoplatelets must be taken into account. Therefore, we use the Xue's equation for carbon nanotube-based composites[40]:

$$3(1-\varphi)\frac{k_{\text{eff}} - k_b}{2\,k_{\text{eff}} + k_b} + \frac{\varphi}{3}\left[\frac{k_{\text{eff}} - k_{p,l}}{k_{\text{eff}} + B\left(k_{p,l} - k_{\text{eff}}\right)} + \frac{2\left(k_{\text{eff}} - k_{p,d}\right)}{k_{\text{eff}}(1-B)\left(k_{p,d} - k_{\text{eff}}\right)}\right] = 0, \tag{9}$$

where $B$ is a dimensionless coefficient depending on the nanoparticle aspect ratio (i.e., $\frac{l}{d}$) and is close to zero for very large aspect ratios, as in our case (see Table III in Appendix A). The longitudinal and transversal thermal conductivities, $k_{p,l}$ and $k_{p,d}$, respectively, are given by:

$$k_{p,l} = \frac{k_p}{1 + \dfrac{2\,R_k\,k_p}{l}}, \tag{10a}$$

$$k_{p,d} = \frac{k_p}{1 + \dfrac{2\,R_k\,k_p}{d}}. \tag{10b}$$

The employed value for the interfacial thermal conductivity of GNPs is $R_K \approx 1 \times 10^{-8}\ \text{m}^2\ \text{K W}^{-1}$, which is taken from non-equilibrium molecular dynamics simulations of few-layer graphene in water.[41]

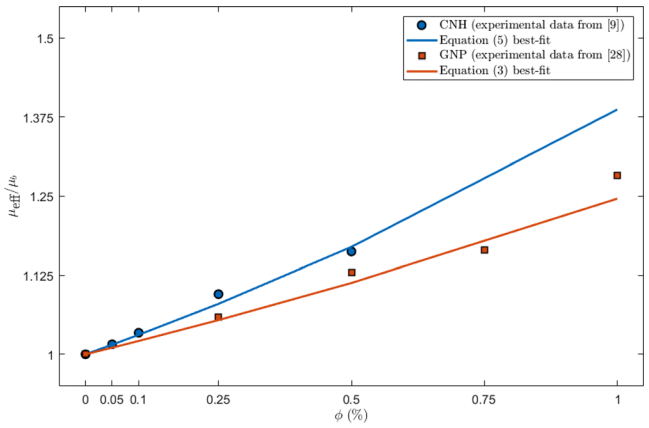


**FIG. 1.** Effective dynamic viscosity of CNH and GNP-based nanofluids: experimental values vs single-phase models.

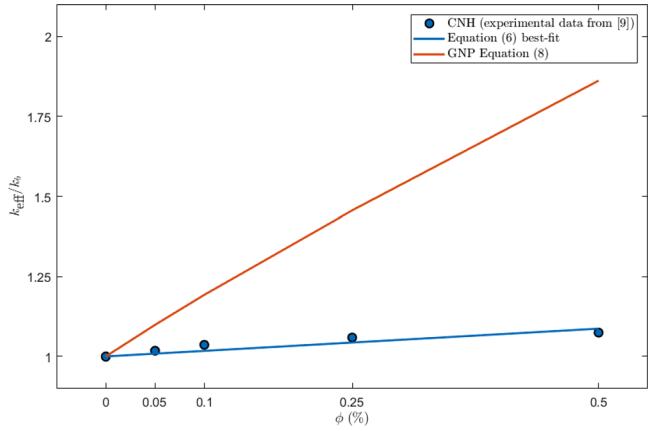


**FIG. 2.** Effective thermal conductivity of CNH and GNP-based nanofluids: experimental values vs single-phase models.

The solution of Eq. (9) is obtained iteratively, and the result is shown in Fig. 2. Due to the extreme in-plane thermal conductivity of graphene, the effective conductivity of the GNP-based nanolubricant is much larger than that computed for the PAG-CNH, up to about 170% for $\varphi = 0.5\%$. Therefore, as we will show more in detail in Sec. III B, the PAG-CNH and the PAG-GNP nanolubricants present a very different behavior in terms of thermal performance. This is due to the difference in the effective thermal conductivity of the nanofluid, which is largely affected by the in-plane conductivity of graphene with respect to quasi-spherical carbon nanoparticles.

### C. Temperature dependence

We assume that each effective property of the nanofluids follows exactly the same temperature dependence of the corresponding property of the base fluid (Table I in Appendix A). In other words, we assume that the ratios $\frac{\rho_{eff}}{\rho_b}$, $\frac{c_{eff}}{c_b}$, $\frac{\mu_{eff}}{\mu_b}$, and $\frac{k_{eff}}{k_b}$ are constant with temperature. We believe this is a good approximation of the actual behavior of the considered nanofluids. In fact, in the typical range of temperature variation of a lubricant (e.g., from ambient temperature to about 100 °C), the properties of the nanoparticles can be considered constant. Instead, the properties of the base fluid can exhibit a strong variation also in a relatively small temperature range, especially in the case of the dynamic viscosity, which is of outmost importance in the determination of the rheological performance of a tribological contact.

## III. CFD SIMULATIONS OF THE CONVECTIVE HEAT TRANSFER

### A. Simulation details

Laminar CFD simulations are carried out in order to evaluate the convective heat transfer properties of the considered nanolubricants; similar approaches have already been followed for single-phase nanofluid models (see, e.g., Ref. 42). The complete set of equations solved is reported in Appendix B.

Here, we consider two infinite parallel plates, with length $L = 2.00$ m and separated by a distance $D = 0.05$ m. The geometry is discretized with a quadrilateral mesh and a mesh convergence study is carried out in order to select the optimal cell size. Considering the variation on the wall temperature $T_{w,\text{out}}$ at the outlet, we choose a mesh of $8000 \times 20$ elements, i.e., with square elements with a side length of 0.25 mm, which allows a tolerance below 0.3% in terms of grid independence.

We apply the following boundary conditions:

- the flow at the inlet has a constant velocity $U = 0.025$ m s$^{-1}$ and a temperature $T_{\text{in}} = 305$ K;
- the pressure at the inlet and at the outlet is set to the atmospheric pressure, i.e., $p_{\text{in}} = p_{\text{out}} = p_{\text{atm}} = 101\,325$ Pa;
- a constant heat flux $q = 1000$ W m$^{-2}$ is applied at the walls;
- no-slip velocity boundary conditions at the walls;
- "outflow" boundary conditions at the outlet.

The corresponding Reynolds number, taking into account the values of the density and dynamic viscosity at the inlet temperature, is $\text{Re} \approx 20$ and, given that $D/L \ll 1$, the flow results both hydrodynamically and thermally fully developed at the outlet.[43]

The Navier–Stokes–Fourier's system of equations is solved with the finite-volume method. A first-order upwind scheme is used to obtain an initial convergence (up to a residual of $10^{-5}$ for continuity and momentum equations and $10^{-6}$ for the energy equation), and then, the result is further refined with a QUICK discretization scheme.[44] The SIMPLEC algorithm is employed here for pressure–velocity coupling.[45]

### B. Convective heat transfer coefficient

The convective heat transfer coefficient is computed as:[43]

$$h(x) = \frac{q}{T_w(x) - T_c(x)}, \tag{11}$$

where $T_c$ is the centerline temperature, $T_w$ is the temperature of the fluid at the wall, and $x$ is the longitudinal coordinate.

Figures 3(a) and 3(b) show the trend of $h$ as a function of the dimensionless coordinate $x/D$ and of the considered volume fractions of nanoparticles, for the PAG-CNH and PAG-GNP nanolubricants, respectively. After the initial transient up to about 30% of the pipe length, the flow becomes thermally fully developed, as anticipated above, and $h$ maintains a constant value. It is possible to quantify the higher effectiveness of graphene nanoplatelets, with respect to carbon nanohorns, in improving the heat transfer performance of the nanofluid. For $\varphi = 0.05\%$, 0.10%, 0.25%, and 0.50%, the asymptotic value

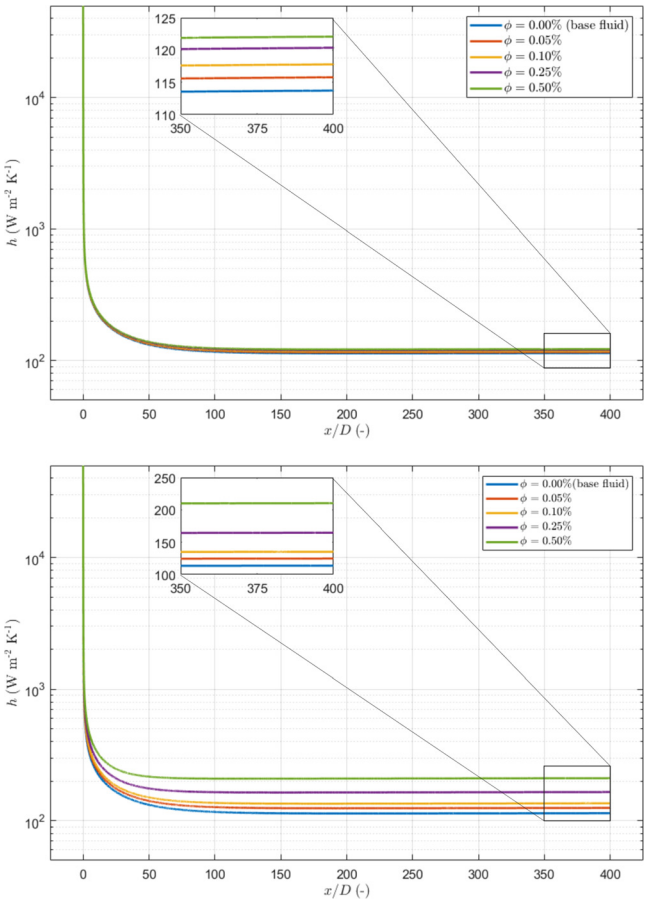


FIG. 3. (a, top) and (b, bottom): Convective heat transfer coefficient as a function of the dimensionless coordinate and of the nanoparticle volume fraction for the PAG-CNH (top) and PAG-GNP (bottom) nanolubricants.

of $h$ results 8%, 15%, 37%, and 72%, respectively, larger for the GNP-based nanofluid.

## IV. CASE STUDY: HYDRODYNAMIC LUBRICATION

### A. Introduction

In this section, we apply the single-phase models for the modeling of the PAG-based nanolubricants introduced above to hydrodynamic lubrication. The objective is to evaluate the heat transfer performance of the considered nanolubricants in the case of a plane slider bearing geometry and also to estimate the effect of nanoparticle volume fraction on some tribological characteristics, namely the load-carrying capacity of the bearing and the overall coefficient of friction.

The fundamental equation of fluid film lubrication was introduced by Reynolds at the end of the 19th century:[46]

$$\frac{\partial}{\partial x}\left(\frac{\rho H^3}{\mu}\frac{\partial p}{\partial x}\right)+\frac{\partial}{\partial y}\left(\frac{\rho H^3}{\mu}\frac{\partial p}{\partial y}\right)=6\,v_x\frac{\partial(\rho H)}{\partial x}, \tag{12}$$

where $H(x)$ is the fluid film thickness, $p(x,y)$ is the pressure field, and $v_x$ is the velocity of the moving wall. The solution of Eq. (12) can be easily derived analytically in the case of constant fluid properties (i.e., $\rho$ and $\mu$).[47] One of the main results that can be obtained from the integration of the Reynolds equation is the pressure variation in the bearing, also known as the load-carrying capacity.

A generalized Reynolds equation with variation of the fluid properties along and across the lubricant film has also been proposed.[48] However, the simultaneous temperature dependence of the density and the viscosity, as well as the variation of the temperature along and across the lubricant film, makes a closed-form solution very difficult to obtain. Therefore, a numerical solution is quicker and more efficient. For this reason, in this work, we employ a CFD approach allowing to consider the temperature-dependent density, specific heat capacity, dynamic viscosity, and thermal conductivity of the nanofluid. Since the main focus of the work is on evaluating the performance of different formulations of nanolubricants, we consider mainly different possible volume fractions of nanoparticles and keep constant all other fluid dynamic parameters (e.g., the Reynolds number), following the setup described in Sec. III A.

### B. Simulation details

In this work, we consider a plane slider bearing and we employ CFD simulations to solve the complete Navier–Stokes–Fourier's system of equations. In this way, it is possible to consider the temperature increase in the fluid due to the viscous heating and thus to take into account the temperature-dependent properties of the nanofluid, as already done in Sec. III A.

The considered geometry, as schematized in Fig. 4, is composed of two convergent surfaces with $H_{\text{in}}=20\,\mu$m, $H_{\text{out}}=10\,\mu$m, $L=10$ mm, and an infinite out-of-plane dimension. The top wall is kept stationary, while the bottom wall slides with a constant velocity $v_x=5$ m s$^{-1}$. The boundary conditions for the pressure are $p_{\text{in}}=p_{\text{out}}=p_{\text{atm}}=101\,325$ Pa, while the inlet temperature is set to $T_{\text{in}}=305$ K. The geometry is discretized with $10\,000\times 14$ quadrilateral cells. The convergence study is not shown here, for brevity, and we use all the discretization schemes described in Sec. III A.

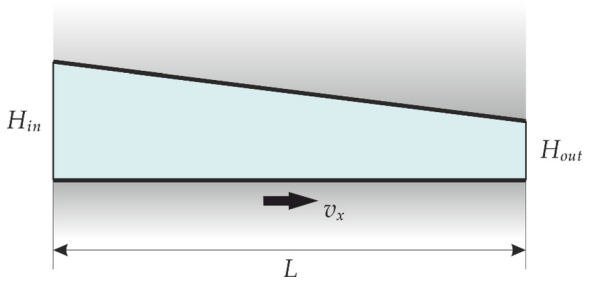


**FIG. 4.** Plane slider bearing geometry and dimensions.

### C. Convective vs adiabatic temperature rise

So far we have demonstrated the superior thermal performance of the PAG-GNP nanolubricant with respect to the PAG-CNH nanolubricant, quantified by the asymptotic value of the convective heat transfer coefficient. Now we make use of the computed values of $h$ as boundary conditions in the plane slider bearing, i.e., the walls are able to extract heat through convection. Note that this is consistent with the previous CFD simulations because two parallel infinite plates have been considered. The obtained mean temperature rise of the lubricant, given by the difference $\Delta T_c = T_{\text{out}} - T_{\text{in}}$ averaged between the moving and the sliding wall, is compared to the mean adiabatic temperature rise $\Delta T_a$, i.e., obtained with adiabatic walls as boundary conditions.

In Fig. 5, the quantity $\Delta T = \Delta T_a - \Delta T_c$, as variation with respect to the case $\varphi = 0.00\%$, is plotted for the two nanolubricants as a function of the nanoparticle volume fraction. We observe that $\Delta T$ increases almost linearly with $\varphi$, with the graphene nanoplatelet-based fluid allowing a heat extraction up to about 60% higher than the PAG-CNH system, for the maximum volume fraction.

### D. Load-carrying capacity and coefficient of friction

The pressure distributions inside the bearing are shown in Figs. 6(a) and 6(b) for the PAG-CNH and the PAG-GNP nanolubricant, respectively. Figure 7, instead, displays the total load-carrying

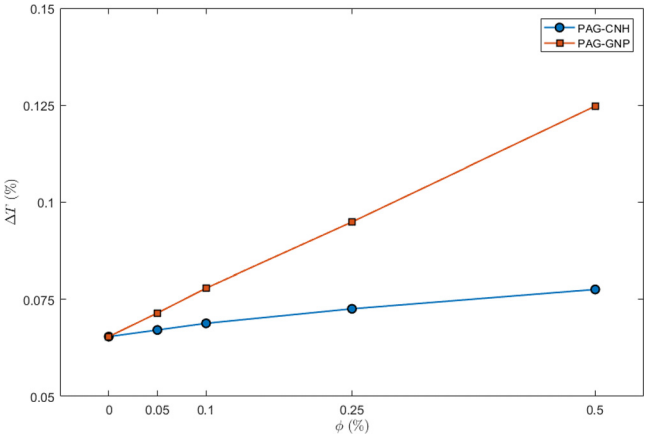


**FIG. 5.** Adiabatic-convective temperature rise difference as a function of the nanoparticle volume fraction for the considered nanolubricants.

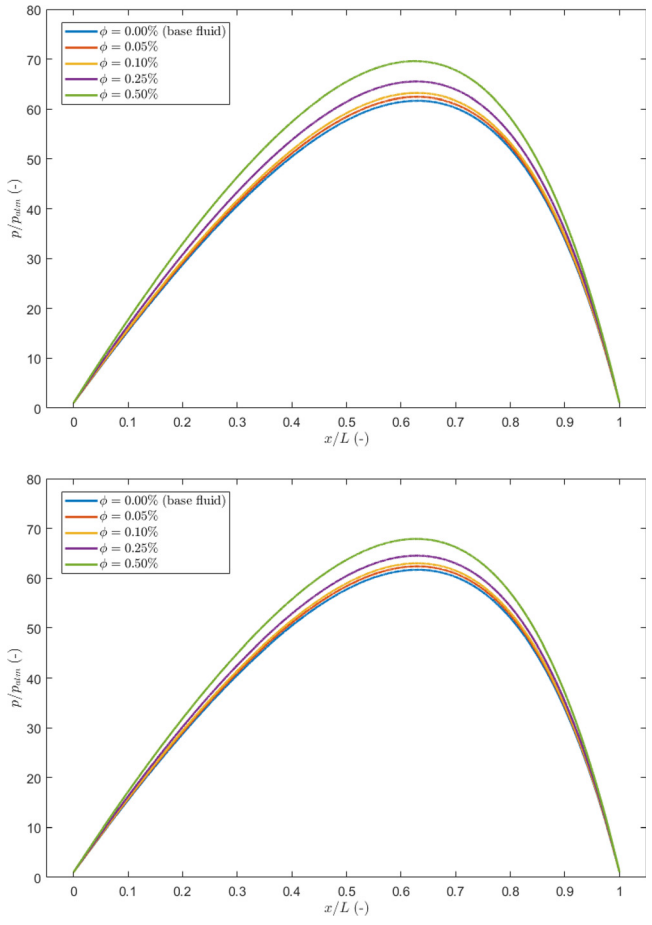


**FIG. 6.** (a, top) and (b, bottom): Pressure distributions inside the bearing as a function of the dimensionless coordinate and of the nanoparticle volume fraction for the PAG-CNH (top) and PAG-GNP (bottom) nanolubricants.

capacity $F_n$, provided by Eq. (14b), as a function of the nanoparticle volume fraction for both nanofluids. The result is very similar for both nanofluids because the pressure in the bearing is mainly dependent on the fluid viscosity (Fig. 1). Accordingly, an increased nanoparticle volume fraction increases the load-carrying capacity of the bearing. The $p(x)$ function shows the typical trend given by the solution of the Reynolds equation but, as stated above, here it is more precise since we are bypassing approximations related to the physical properties. In addition, the concomitant effect of viscosity increase due to an increasing nanoparticle volume fraction and the viscosity reduction due to an increasing temperature slightly moves the location of the pressure peak toward the inlet for an increasing $\varphi$.

In principle, it is possible to compute the coefficient of friction of the considered bearing through the ratio:[47]

$$f = \frac{F_t}{F_n}, \tag{13}$$

where $F_t$ and $F_n$ are the tangential and the normal force per unit width, respectively, and are given by the integrals:

$$F_t = \int_0^L \tau_w \, dx, \tag{14a}$$

$$F_n = \int_0^L [p(x) - p_{\text{atm}}] \, dx, \tag{14b}$$

where $\tau_w$ is the shear stress at the wall.

In Fig. 8, we plot the variation $\Delta f$ of the coefficient of friction as a function of $\varphi$ for the considered nanolubricants, with respect to the base fluid. As expected, $f$ decreases for an increasing nanoparticle volume fraction, mainly due to the increase in the load-carrying capacity displayed in Fig. 7. However, the variation with respect to the base fluid is very small if compared to the experimental data reported in the literature. We believe that this can be attributed to the fact that in general the optimal tribological performance of a nanofluid is observed in the regime of boundary or mixed lubrication, where there is an increase in the load-carrying capacity due to the presence of dispersed hard nanoparticles. Additionally, the nanoparticles can also interact

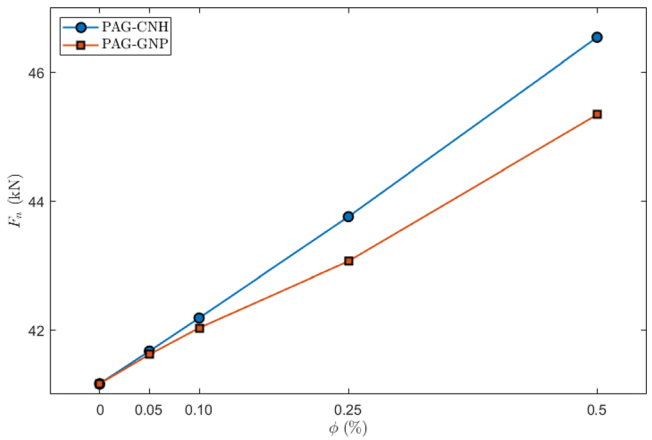


**FIG. 7.** Load-carrying capacity of the bearing computed through Eq. (14b) as variation with respect to the case of the base fluid, as a function of the nanoparticle volume fraction for the considered nanolubricants.

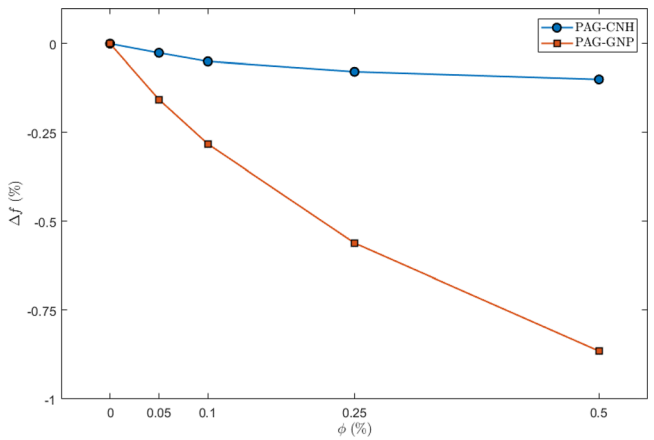


**FIG. 8.** Coefficient of friction computed through Eq. (13) as variation with respect to the case of the base fluid, as a function of the nanoparticle volume fraction for the considered nanolubricants.

with the surface roughness. Here, the considered case of hydrodynamic lubrication and the use of single-phase models do not allow to highlight these phenomena, but a general trend in reducing friction is retrieved.

## V. CONCLUSIONS

In this paper, we have applied single-phase models to graphene-based nanolubricants, in order to evaluate their heat transfer properties by means of CFD simulations with temperature-dependent properties. We have shown how the physical properties of the nanoparticles have a great impact on the overall thermal properties of the nanofluid: thanks to the high in-plane thermal conductivity of the GNPs, we have quantified the increase in convective heat transfer coefficient of the related nanolubricant with respect to the PAG-CNH system.

In addition, to the best of our knowledge, this work represents the first application of single-phase nanofluid models to hydrodynamic lubrication. Also in this case, the thermal conductivity of the nanoparticles plays a fundamental role, affecting the temperature rise of the fluid. Conversely, the viscosity of the nanolubricant affects the load-carrying capacity and the coefficient of friction of the bearing, which we have computed as a function of the nanoparticle volume fraction. Despite viscosity index improvers and/or polymer thickeners are also available in industry and in technical literature, the use of nanofluid-based lubricants brings significant benefits, above all in terms of efficient heat dissipation, precise viscosity tuning (also as a function of temperature), and reduced wear of the contacting surfaces.

We believe the results of the present work can provide useful insight for the development of novel and high-performance carbon-based nanolubricants. Future research should be addressed to the investigation of mixed or boundary lubrication regimes, where the nanoparticles can be more effective from the tribological point of view, by employing more advanced modeling techniques. In this case, indeed, a single-phase model should be overcome in order to take into account potential contacts within solids.[50] The experimental validations in example applications should be considered within future research efforts, with special emphasis on optimized nanofluid formulations for low-wear and low-friction applications.

Another interesting field of application of the proposed approach is represented by nano- and microscale-engineered fluids with specific magnetic properties, whose research efforts have been centered so far on the modulation of the ferrofluid dynamics toward achieving augmented fluidic functionalities.[51–54]

## AUTHOR DECLARATIONS

### Conflict of Interest

The authors have no conflicts to disclose.

### Author Contributions

**Roberto Guarino:** Conceptualization (equal); Formal analysis (equal); Methodology (equal); Writing – original draft (equal); Writing – review & editing (equal). **Nicola Maria Pugno:** Funding acquisition (equal); Supervision (equal); Writing – review & editing (equal).

## DATA AVAILABILITY

The data that support the findings of this study are available from the corresponding author upon reasonable request.

## APPENDIX A: BASE FLUID AND NANOPARTICLE PROPERTIES

**TABLE I.** Temperature-dependent physical properties of the considered base fluid (from Refs. 26–28]).

| $T$ (K) | $\rho$ (kg m$^{-3}$) | $c$ (J kg$^{-1}$ K$^{-1}$) | $\mu$ (Pa s) | $k$ (W m$^{-1}$ K$^{-1}$) |
|---|---|---|---|---|
| 293 | 1000.0 | 1933.4 | 0.0973 | 0.1480 |
| 303 | 992.0 | 1966.7 | 0.0689 | 0.1475 |
| 313 | 984.0 | 2000.0 | 0.0489 | 0.1470 |
| 323 | 976.0 | 2033.3 | 0.0346 | 0.1465 |
| 333 | 968.0 | 2066.6 | 0.0246 | 0.1460 |
| 343 | 960.0 | 2099.9 | 0.0174 | 0.1455 |
| 353 | 952.0 | 2133.2 | 0.0123 | 0.1450 |
| 363 | 944.0 | 2166.5 | 0.0088 | 0.1445 |
| 373 | 936.0 | 2199.8 | 0.0062 | 0.1440 |

**TABLE II.** Physical properties of the considered CNHs at $T = 298$ K (from Ref. 32).

| Property | Value |
|---|---|
| $\rho$ | 500.0 kg m$^{-3}$ |
| $c$ | 800.0 J kg$^{-1}$ m$^{-1}$ |
| $r$ | 40.0 nm |

**TABLE III.** Physical properties of the considered GNPs at $T = 298$ K (from Ref. 33).

| Property | Value |
|---|---|
| $\rho$ | 100.0 kg m$^{-3}$ |
| $c$ | 800.0 J kg$^{-1}$ m$^{-1}$ |
| $k$ | 3000.0 W m$^{-1}$ K$^{-1}$ |
| $l$ | 2000 nm |
| $d$ | 2 nm |

## APPENDIX B: CFD SYSTEM OF EQUATIONS

The governing equations of the fluid flow describe the fundamental principles of mass, momentum, and energy conservations, which are given, respectively, by

$$\frac{\partial \rho}{\partial t} + \nabla \cdot (\rho \boldsymbol{U}) = 0, \tag{B1}$$

$$\rho \frac{D\boldsymbol{U}}{Dt} = -\nabla p + \nabla \cdot \boldsymbol{\tau} + \rho \boldsymbol{g}, \tag{B2}$$

$$\rho \frac{De}{Dt} + p(\nabla \cdot \boldsymbol{U}) = \frac{\partial Q}{\partial t} - \nabla \cdot \boldsymbol{q} + \boldsymbol{\Phi}, \tag{B3}$$

where $\boldsymbol{U}$ is the fluid velocity, $\boldsymbol{\tau}$ is the viscous stress tensor, $\boldsymbol{g}$ is the body force tensor (here of inertia), $e$ is the energy, $Q$ is the heat source term, $\nabla \cdot \boldsymbol{q}$ is the heat loss by conduction (given by the Fourier's law), and $\boldsymbol{\Phi}$ is a dissipative term.

In the general case, the solution of the Eqs. (B1)–(B3) requires a numerical technique. In this work, we employ the finite-volume method, which is the most popular method used in CFD simulations and is implemented in several commercial and open-source codes. The details of the discretization and the numerical solution (including a treatment on numerical stability) can be found in the specialized literature.[49]

With reference to the CFD simulation of the plane slider bearing reported in Sec. IV B, we implement the following boundary conditions:

- an inlet pressure equal to the ambient pressure (i.e., $p_{in} = p_{atm} = 101\,325$ Pa);
- an outlet pressure, again, equal to the ambient pressure (i.e., $p_{out} = p_{atm} = 101\,325$ Pa);
- a no-slip velocity boundary conditions on the walls of the bearing;
- a constant $x$-velocity of the bottom wall of the bearing equal to $v_x = 5\ \mathrm{m\ s^{-1}}$, which transfers the motion to the surrounding fluid;
- an inlet temperature equal to the ambient temperature (i.e., $T_{in} = 305$ K);
- "outflow" boundary conditions at the outlet for both temperature and velocity;
- a zero wall heat flux, so that the heating of the fluid and the temperature rise are only given to the viscous (i.e., frictional) dissipation.

The numerical procedure, in brief, involves the following consecutive steps:

(1) creation of the geometry and import into the solver;
(2) creation of the mesh according to the chosen discretization;
(3) numerical solution of the Eqs. (B1)–(B3) by means of the solver and by employing a second-order upwind scheme;
(4) extraction of the basic quantities (i.e., fluid flow velocity and temperature) for each mesh element;
(5) integration of the basic quantities to obtain derived quantities, such as mass flow rates, pressures, and shear stresses;
(6) offline calculation of the overall forces according to Eqs. (14) and of the coefficient of friction of the bearing according to Eq. (13).

## REFERENCES


[1]G. Paul, H. Hirani, T. Kuila, and N. C. Murmu, "Nanolubricants dispersed with graphene and its derivatives: An assessment and review of the tribological performance," Nanoscale **11**, 3458–3483 (2019).
[2]G. Paul, S. Shit, H. Hirani, T. Kuila, and N. C. Murmu, "Tribological behavior of dodecylamine functionalized graphene nanosheets dispersed engine oil nanolubricants," Tribol. Int. **131**, 605–619 (2019).
[3]M. K. A. Ali, H. Xianjun, M. A. A. Abdelkareem, M. Gulzar, and A. H. Elsheikh, "Novel approach of the graphene nanolubricant for energy saving via anti-friction/wear in automobile engines," Tribol. Int. **124**, 209–229 (2018).
[4]J. A. C. Cornelio, P. A. Cuervo, L. M. Hoyos-Palacio, J. Lara-Romero, and A. Toro, "Tribological properties of carbon nanotubes as lubricant additive in oil and water for a wheel–rail system," J. Mater. Res. Technol. **5**(1), 68–76 (2016).
[5]A. K. Rasheed, M. Khalid, A. Javeed, W. Rashmi, T. C. S. M. Gupta, and A. Chan, "Heat transfer and tribological performance of graphene nanolubricant in an internal combustion engine," Tribol. Int. **103**, 504–515 (2016).
[6]A. I. Vakis, V. A. Yastrebov, J. Scheibert, L. Nicola, D. Dini, C. Minfray, A. Almqvist, M. Paggi, S. Lee, G. Limbert, J. F. Molinari, G. Anciaux, R. Aghababaei, S. Echeverri Restrepo, A. Papangelo, A. Cammarata, P. Nicolini, C. Putignano, G. Carbone, S. Stupkiewicz, J. Lengiewicz, G. Costagliola, F. Bosia, R. Guarino, N. M. Pugno, M. H. Müser, and M. Ciavarella, "Modeling and simulation in tribology across scales: An overview," Tribol. Int. **125**, 169–199 (2018).
[7]N. Kumar and P. Goyal, "Experimental study of carbon nanotubes to enhance tribological characteristics of lubricating engine oil SAE10W40," IOP Conf. Ser.: Mater. Sci. Eng. **1225**, 012052 (2022).
[8]A. Senatore, H. Hong, V. D'urso, and H. Younes, "Tribological behavior of novel CNTs-based lubricant grease in steady-state and fretting sliding conditions," Lubricants **9**(11), 107 (2021).
[9]V. Zin, S. Barison, F. Agresti, L. Colla, C. Pagura, and M. Fabrizio, "Improved tribological and thermal properties of lubricants by graphene based nano-additives," RSC Adv. **6**(64), 59477–59486 (2016).
[10]Y. B. Guo and S. W. Zhang, "The tribological properties of multi-layered graphene as additives of $PAO_2$ oil in steel-steel contacts," Lubricants **4**(3), 30 (2016).
[11]S. Liang, Z. Shen, M. Yi, L. Liu, X. Zhang, and S. Ma, "In-situ exfoliated graphene for high-performance water-based lubricants," Carbon **96**, 1181–1190 (2016).
[12]M. G. Ivanov and D. M. Ivanov, "Nanodiamond nanoparticles as additives to lubricants," in *Ultrananocrystalline Diamond: Synthesis, Properties and Applications*, edited by O. A. Shenderova and D. M. Gruen (Elsevier, 2012).
[13]A. K. Rasheed, M. Khalid, W. Rashmi, T. C. S. M. Gupta, and A. Chan, "Graphene based nanofluids and nanolubricants—Review of recent developments," Renewable Sustainable Energy Rev. **63**, 346–362 (2016).
[14]A. Mescola, G. Paolicelli, S. P. Ogilvie, R. Guarino, J. G. McHugh, A. Rota, E. Iacob, E. Gnecco, S. Valeri, N. M. Pugno, V. Gadhamshetty, M. M. Rahman, P. Ajayan, A. B. Dalton, and M. Tripathi, "Graphene confers ultralow friction on nanogear cogs," Small **17**, 2104487 (2021).
[15]P. Kumar Tyagi, R. Kumar, and P. Kumar Mondal, "A review of the state-of-the-art nanofluid spray and jet impingement cooling," Phys. Fluids **32**, 121301 (2020).
[16]A. Gogoi, K. Anki Reddy, and P. Kumar Mondal, "Influence of the presence of cations on the water and salt dynamics inside layered graphene oxide (GO) membranes," Nanoscale **12**, 7273–7283 (2020).
[17]S. Kumar Mehta and P. Kumar Mondal, "Free convective heat transfer and entropy generation characteristics of the nanofluid flow inside a wavy solar power plant," Microsystem Technol. **29**, 489–500 (2022).
[18]R. Sarma, A. Kumar Shukla, H. S. Gaikwad, P. Kumar Mondal, and S. Wongwises, "Effect of conjugate heat transfer on the thermo-electro-hydrodynamics of nanofluids: Entropy optimization analysis," J. Therm. Anal. Calorimetry **147**, 599–614 (2022).
[19]A. Kamyar, R. Saidur, and M. Hasanuzzaman, "Application of Computational Fluid Dynamics (CFD) for nanofluids," Int. J. Heat Mass Transfer **55**(15–16), 4104–4115 (2012).
[20]S. Göktepe, K. Atalik, and H. Ertürk, "Comparison of single and two-phase models for nanofluid convection at the entrance of a uniformly heated tube," Int. J. Therm. Sci. **80**(1), 83–92 (2014).
[21]S. Kakaç and A. Pramuanjaroenkij, "Single-phase and two-phase treatments of convective heat transfer enhancement with nanofluids—A state-of-the-art review," Int. J. Therm. Sci. **100**, 75–97 (2016).
[22]A. Einstein, "Eine neue Bestimmung der Molekuldimensionen," Annalen der Phys. **324**, 289–306 (1906).
[23]A. Amiri, H. K. Arzani, S. N. Kazi, B. T. Chew, and A. Badarudin, "Backward-facing step heat transfer of the turbulent regime for functionalized graphene nanoplatelets based water–ethylene glycol nanofluids," Int. J. Heat Mass Transfer **97**, 538–546 (2016).
[24]A. R. Khaliq, R. Kafafy, H. M. Salleh, and W. F. Faris, "Enhancing the efficiency of polymerase chain reaction using graphene nanoflakes," Nanotechnology **23**(45), 455106 (2012).
[25]H. Shahmohamadi, R. Rahmani, H. Rahnejat, C. P. Garner, and N. Balodimos, "Thermohydrodynamics of lubricant flow with carbon nanoparticles in tribological contacts," Tribol. Int. **113**, 50–57 (2017).
[26]W. H. Millett, "Polyalkylene glycol synthetic lubricants," Ind. Eng. Chem. **42**(12), 2436–2441 (1950).

[27]E. R. Mueller and M. H. William, "Polyalkylene glycol lubricants: Uniquely water soluble," Lubrication Eng. **31**(7), 348–356 (1975).
[28]S. Komatsuzaki, Y. Homma, K. Kawashima, and Y. Itoh, "Polyalkylene glycol as lubricant for HFC-134a compressors," Lubrication Eng. **47**(12), 1018–1025 (1991).
[29]S. Lawford, "Polyalkylene glycols," in *Synthetics, Mineral Oils, and Bio-Based Lubricants*, edited by L. R. Rudnick (CRC Press, 2006).
[30]X. Liu, N. Xu, M. Zhang, L. Chen, W. Lou, and X. Wang, "Exploring the effect of nanoparticle size on the tribological properties of $SiO_2$/polyalkylene glycol nanofluid under different lubrication conditions," Tribol. Int. **109**, 467–472 (2017).
[31]M. Z. Sharif, W. H. Azmi, A. A. M. Redhwan, and R. Mamat, "Investigation of thermal conductivity and viscosity of $Al_2O_3$/PAG nanolubricant for application in automotive air conditioning system," Int. J. Refrigeration **70**, 93–102 (2016).
[32]N. Karousis, I. Suarez-Martines, C. P. Ewels, and N. Tagmatarchis, "Structure, properties, functionalization, and applications of carbon nanohorns," Chem. Rev. **116**(8), 4850–4883 (2016).
[33]M. Mehrali, E. Sadeghinezhad, S. T. Latibari, S. N. Kazi, M. Mehrali, M. N. B. M. Zubir, and H. S. C. Metselaar, "Investigation of thermal conductivity and rheological properties of nanofluids containing graphene nanoplatelets," Nanoscale Res. Lett. **9**(1), 15 (2014).
[34]S. H. Maron and P. E. Pierce, "Application of Ree-Eyring generalized flow theory to suspensions of spherical particles," J. Colloid Sci. **11**, 80–95 (1956).
[35]H. Chen, Y. Ding, and C. Tan, "Rheological behaviour of nanofluids," New J. Phys. **9**, 367 (2007).
[36]S. Halelfadl, P. Estellé, B. Aladag, N. Doner, and T. Maré, "Viscosity of carbon nanotubes water-based nanofluids: Influence of concentration and temperature," Int. J. Therm. Sci. **71**, 111–117 (2013).
[37]C.-W. Nan, Z. Shi, and Y. Lin, "A simple model for thermal conductivity of carbon nanotube-based composites," Chem. Phys. Lett. **375**(5–6), 666–669 (2003).
[38]C.-W. Nan, G. Liu, Y. Lin, and M. Li, "Interface effect on thermal conductivity of carbon nanotube composites," Appl. Phys. Lett. **85**(16), 3549–3551 (2004).
[39]C. Selvam, S. Harish, and D. M. Lal, "Effective thermal conductivity and rheological characteristics of ethylene glycol-based nanofluids with single-walled carbon nanohorn inclusions," Fullerenes Nanotubes Carbon Nanostruct. **25**(2), 86–93 (2017).
[40]Q. Xue, "Model for the effective thermal conductivity of carbon nanotube composites," Nanotechnology **17**(6), 1655–1660 (2006).
[41]D. Alexeev, J. Chen, J. H. Walther, K. P. Giapis, P. Angelikopoulos, and P. Komoutsakos, "Kapitza resistance between few-layer graphene and water: Liquid layering effects," Nano Lett. **15**(9), 5744–5749 (2015).
[42]M. K. Moraveji, M. Darabi, S. M. H. Haddad, and R. Davamejad, "Modeling of convective heat transfer of a nanofluid in the developing region of tube flow with computational fluid dynamics," Int. Commun. Heat Mass Transfer **38**(9), 1291–1295 (2011).
[43]A. Bejan, *Convection Heat Transfer* (John Wiley & Sons, Inc., Hoboken, NJ, 2013).
[44]B. P. Leonard, "A stable and accurate convective modelling procedure based on quadratic upstream interpolation," Comput. Methods Appl. Mech. Eng. **19**(1), 59–98 (1979).
[45]J. P. Van Doormaal and G. D. Raithby, "Enhancements of the SIMPLE method for predicting incompressible fluid flows," Numer. Heat Transfer **7**(2), 147–163 (1984).
[46]O. Reynolds, "I. On the theory of lubrication and its application to Mr. Beauchamp tower's experiments, including an experimental determination of the viscosity of olive oil," Philos. Trans. R. Soc. **40**(242–245), 191–203 (1886).
[47]B. J. Hamrock, S. R. Schmid, and B. O. Jacobson, *Fundamentals of Fluid Film Lubrication*, 2nd ed. (Marcel Dekker, New York, 2004).
[48]D. Dowson, "A generalized Reynolds equation for fluid-film lubrication," Int. J. Mech. Sci. **4**, 159–170 (1962).
[49]J. H. Ferziger, M. Peric, and R. L. Street, *Computational Methods for Fluid Dynamics* (Springer, Cham, Switzerland, 2020).
[50]R. Guarino, G. Costagliola, F. Bosia, and N. M. Pugno, "Evidence of friction reduction in laterally-graded materials," Beilstein J. Nanotechnol. **9**, 2443–2456 (2018).
[51]S. Shyam, U. Banerjee, P. K. Mondal, and S. K. Mitra, "Impact dynamics of ferrofluid droplet on a PDMS substrate under the influence of magnetic field," Colloids Surf. A: Physicochem. Eng. Aspects **661**, 130911 (2023).
[52]S. Shyam, B. Dapola, and P. K. Mondal, "Magnetofluidic-based controlled droplet breakup: Effect of non-uniform force field," J. Fluid Mech. **944**, A51 (2022).
[53]N. Nair, S. Shyam, P. K. Mondal, and S. P. Bhatnagar, "Probing into the drying pattern dynamics of a ferrofluid droplet under the actuation of magnetic field," IEEE Trans. Magn. **59**(1), 1–7 (2023).
[54]S. Shyam, A. Yadav, Y. Gawade, B. Mehda, P. K. Mondal, and M. Asfer, "Dynamics of a single isolated ferrofluid plug inside a micro-capillary in the presence of externally applied magnetic field," Exp. Fluids **61**, 210 (2020).